ACS APPLIED MATERIALS & INTERFACES

Research Article

www.acsami.org

Methyl/Allyl Monolayer on Silicon: Efficient Surface Passivation for Silicon-Conjugated Polymer Hybrid Solar Cell

Fute Zhang, Dong Liu, Yunfang Zhang, Huaixin Wei, Tao Song, and Baoquan Sun*

Jiangsu Key Laboratory for Carbon-Based Functional Materials & Devices, Institute of Functional Nano & Soft Materials (FUNSOM), Soochow University, 199 Ren'ai Road, Suzhou, 215123, China

Supporting Information

ABSTRACT: We demonstrate a hybrid Schottky junction solar cell based on methyl/allyl groups terminated silicon nanowire arrays (SiNWs) and poly(3,4-ethylenedioxythiophene)/poly(styrenesulfonate) with a power conversion efficiency (PCE) of 10.2%. The methyl/allyl organic monolayer on silicon can act as an excellent passivation layer for suppressing surface charge recombination, which is characterized by grazing angle attenuated total reflectance Fourier-transform infrared spectroscopy and X-ray photoelectron spectroscopy measurements. The transient and steady electric output characteristics measurements indicate that the density of trap states of SiNWs are dramatically suppressed by methyl/allyl surface modification. In addition, the device based on methyl/allyl passivated SiNWs exhibits improved stable electrical output over those based on either methyl or allyl passivated ones. The improved PCE and good stability of the device are ascribed to efficient functionalization of the SiNW surface.

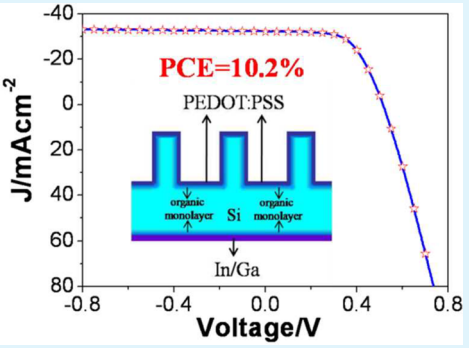

KEYWORDS: *silicon nanowire arrays, organic monolayer, surface passivation, hybrid Schottky solar cell, charge recombination*

1. INTRODUCTION

Up to now, commercial photovoltaic industries are dominated by silicon based productions because of its high power conversion efficiency (PCE) and mature fabrication processes. In addition, silicon, which exhibits nontoxicity, high abundance, and strong optical absorption, provides the most feasibility to replace traditional nonrenewable power consumed worldwide.[1] However, the currently high cost of silicon cells as compared to traditional fossil fuel power source makes it difficult to be widely used.[2] The high cost originates from the consumption of large amounts of high-purity silicon materials as well as the complicated fabrication process. Therefore, reducing the quality and quantity of silicon can help to cut the cost of the silicon cells.

Hybrid solar cells based on conjugated molecules and silicon substrates, which generate a possibility to fabricating cells by solution processes with inexpensive materials, display the potential to be low-cost for solar conversions.[3−9] However, the planar silicon substrates exhibited high reflectivity, which leading to low short-circuit current density (J_{sc}) of planar silicon based devices. Using silicon nanowire arrays (SiNWs) with efficient light trapping and harvesting can overcome this issue effectively. Poly(3,4-ethylenedioxythiophene)/poly-(styrenesulfonate) (PEDOT:PSS) has been widely used in this kind of hybrid solar cells because of its water-soluble, good film-forming properties, high conductivity, high visible light transmissivity and excellent stability.[10,11] Hybrid solar cells composed of SiNWs and PEDOT:PSS have been developed recently with PCE up to 10%.[12−17]

The silicon surface termination state plays key role on the electrical output of the hybrid devices. The hydrogen-terminated silicon surface exhibits a large density of trap states.[3] In the traditional silicon cells, thin SiO_x layer grown by thermal oxidation is utilized to suppress the recombination velocity.[2] However, the thickness of the SiO_x layer gradually increases over time, and the thicker SiO_x eventually becomes a charge injection/transport barrier, resulting in deteriorating the device performance, which is not compatible for the hybrid solar cells.[3,4] An alternative method to avoid SiO_x formation is an organic monolayer bonded covalently to silicon surface, which has been verified an effective passivation layer for the hybrid solar cells. The organic molecules monolayer can be anchored on silicon surface by various techniques. Methyl group has been widely used for silicon surface modification because of its high coverage ratio (more than 90%).[18−21] Whatever the maximum ratio of Si−C bonds, it is clear that a number of uncovered Si−H sites still remain on the surface. Therefore, the Si−H sites are vulnerable to oxidation by water and oxygen. Allyl group has been investigated that it attached on silicon surface easily and provided a highly stable organic monolayer modification.[20,22] In addition, the C=C bond is conjugated so as to benefit for charge transfer. Furthermore, allyl group shows strong electronegativity compared with the methyl group, which provides a larger surface dipole leading to

Received: November 29, 2012
Accepted: May 1, 2013
Published: May 1, 2013

a larger driving force promoting electron movement toward the cathode.[23] However, such surfaces show a large number of incomplete coverage of silicon atop sites, as well as more inferior oxidation resistance and larger electronic defect densities than methyl-terminated ones. To address this issue, researchers have developed hybrid methyl/allyl groups to terminate the planar silicon substrate.[24] The methyl/allyl passivated silicon maintains the chemical stability and electronic properties.

In this work, hybrid Schottky diodes based on methyl/allyl group-terminated SiNWs and PEDOT:PSS are constructed for high-performance solar cells. SiNWs on the planar silicon substrates can be fabricated by a simple process at low temperature. SiNWs are terminated with methyl/allyl groups that act as the passivation layer. Grazing angle attenuated total reflectance Fourier-transform infrared spectroscopy (GATR-FTIR) and X-ray photoelectron spectroscopy (XPS) indicate that methyl/allyl can be anchored onto silicon substrate effectively. Hybrid devices based on SiNWs and PEDOT:PSS achieved a PCE of 10.2% under irradiation with a simulated air mass (AM) 1.5 solar spectrum at 100 mW cm^{-2}. Furthermore, the device fabricated from hybrid methyl/allyl groups passivated SiNWs shows negligible decay in PCE after operation for 240 h. The efficient functionalization of the silicon surface led to the improved PCE and good stability of these devices.

2. EXPERIMENTAL SECTION

2.1. Preparation of SiNWs. SiNWs on planar silicon substrates were prepared by metal ion-assisted electroless etching.[25] Clean n-type silicon substrates (resistivity of ~5 Ω cm) were immersed in an aqueous solution of HF (4.8 M) and $AgNO_3$ (0.02 M) for 20 min at room temperature. After etching, the substrates were dipped into an aqueous solution of HNO_3 (30% w/w) and then rinsed with deionization (DI) water to remove any residual silver.

2.2. Surface Modification. *2.2.1. Hydrogen-Terminated SiNWs.* Hydrogen-terminated SiNWs were prepared by wet chemical etching in aqueous HF (5 M) with gentle shaking for 15 min to remove silicon oxide. Then they were immersed in DI water for 1 min and dried under a stream of N_2 gas. The hydrogen-terminated SiNWs were immediately transferred into glovebox. The SiNWs samples were immersed in a hot saturated solution of PCl_5 in chlorobenzene (CB) at 100 ± 10 °C for 2 h. After this process, the substrates were rinsed with hot CB. Meanwhile, the Si−H surfaces were replaced with Si−Cl ones.

2.2.2. Organic Surface Modification. Freshly prepared chlorine terminated SiNWs substrates were immersed in a solution of CH_3MgCl (1 M) (CH_2CHCH_2MgCl, 1 M) in tetrahydrofuran (THF) for at least 8 h at 70 ± 10 °C (24 h at 100 ± 10 °C) and then rinsed with THF to obtain methyl (allyl)-terminated silicon substrate. For methyl/allyl-terminated SiNWs, chlorine-terminated SiNWs substrates were immersed in the solution of CH_2CHCH_2MgCl (1 M) in THF for at least 24 h at 100 ± 10 °C and then rinsed with THF, then the substrates were immersed in the solution of CH_3MgCl (1 M) in THF for at least 8 h at 70 ± 10 °C and rinsed with THF. The samples were taken out of the glovebox, immersed in methanol for 30 min, and then rinsed sequentially with acetone, ethanol, and DI water.

2.3. Characterization of Organic Monolayer Passivated SiNWs. The organic monolayer modified SiNWs surfaces were characterized by XPS (Shimadzu ESCA-1000 spectrometer and a KRATOS-AXIS-165 spectrometer using a Mg KR line), GATR-FTIR (Bruker Optics, VERTEX 70, Ge crystal angle attenuated total reflectance) measurements, respectively.

2.4. Device Fabrication and Characterization. PEDOT:PSS film was deposited onto the SiNWs substrate by spin-coating an aqueous solution of PEDOT:PSS (CLEVIOS PH 1000). A wetting agent of Trion X-100 was added to the PEDOT:PSS solution, which help the wetting property of PEDOT:PSS on the organic terminated SiNWs. The substrate coated with PEDOT:PSS film was baked at 110 °C in nitrogen for 10 min. Then a silver grid electrode was deposited onto PEDOT:PSS layer. Finally, indium−gallium alloy (In/Ga) was attached onto the rear side of the substrate for back contact. The edges of the device were covered with stainless steel mask and the area for illumination was 1 cm ×0.8 cm which was shown in Figure S1 in the Supporting Information. A Newport 91160 solar simulator equipped with a 300 W xenon lamp and an AM 1.5 filter was used as an irradiation source to generate a simulated solar spectrum. The irradiation intensity was 100 mW cm^{-2}, which was calibrated by a standard silicon photovoltaic device (91150, Newport).

3. RESULTS AND DISCUSSION

3.1. Silicon Surface Characterization. The methyl/allyl groups on silicon are characterized by GATR-FTIR and XPS measurements. Figure 1 shows representatives spectra of the three surface passivations prepared from two-step chlorination/alkylation method. The methyl-terminated silicon surface shows only one peak at 1263 cm^{-1}, which is ascribed to methyl group vibrational mode. For the allyl-terminated silicon surface, only one peak at 1650 cm^{-1} is observed, which can be assigned to allyl vibrational mode. For methyl/allyl-terminated silicon surface, two peaks at 1263 and at 1650 cm^{-1} are observed, respectively. Compared with methyl terminated silicon surface, the intensity of methyl vibrational mode at 1263 cm^{-1} is weak. Compared with allyl terminated silicon surface, the intensity of allyl vibrational mode at 1650 cm^{-1} decreased. It means that the Si−H sites at the silicon surface are replaced by both methyl and allyl groups. In addition, the absolute intensities in GATR-FTIR spectra are not very precise for quantitative coverage determination, because the peak

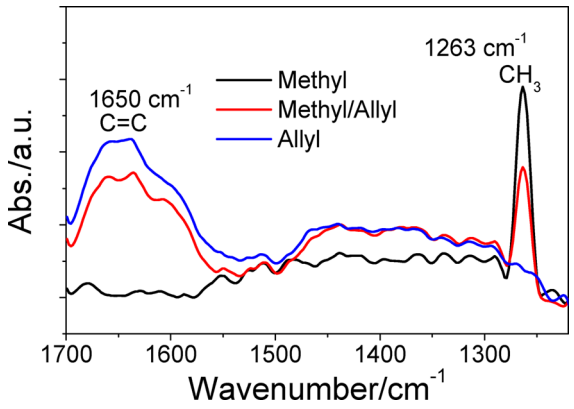

Figure 1. GATR-FTIR spectra of different surface termination methods (methyl, ally, and methyl/ally) on planar silicon.

dx.doi.org/10.1021/am302893r | ACS Appl. Mater. Interfaces 2013, 5, 4678−4684

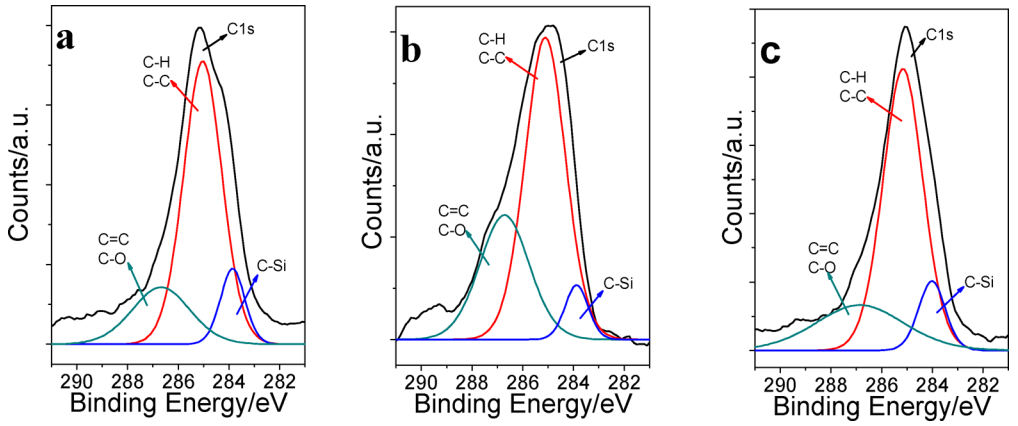

Figure 2. XPS of C1s region, showing C−Si, C−C and C−H, and C−O and C═C for freshly prepared organic monolayer terminated SiNWs. The C−O signal arises from adventitious carbonaceous material and does not indicate the formation of SiO_x or alkoxides. (a) Methyl-terminated SiNWs; (b) allyl-terminated SiNWs; (c) methyl/allyl-terminated SiNWs.

intensities are sensitive to the contact between the sample and the germanium crystal.

The surface termination ratio by various groups can be estimated by XPS measurement. Generally, the ratio is terminated by Γ_{Si-C} and Γ_{Si}, where Γ_{Si-C} is the number of Si−C bonds per area unit, and Γ_{Si} is the number of the total silicon bonds per area unit. The ratio can be calculated by $\Gamma_{Si-C}/\Gamma_{Si}$. Figure 2 shows XPS data from the C_{1s} emission region of the different organic groups terminated SiNWs, fitted to three peaks: C−Si at 283.85 ± 0.05 eV, C−C and C−H at 285.10 ± 0.05 eV, C−O and C═C at 286.75 ± 0.05 eV. The values of $\Gamma_{Si-C}/\Gamma_{Si}$ are summarized in Table 1. The results

Table 1. Summary of the XPS Results of SiNWs with the Different Surface Passivations

surface	$\Gamma_{Si-C}/\Gamma_{Si}$	coverage ratio (%)
methyl-SiNWs	0.0219 ± 0.001	90
allyl-SiNWs	0.0144 ± 0.001	59.2 ± 0.5
methyl/allyl-SiNWs	0.0241 ± 0.001	99.2 ± 0.5

indicate that more than 90% of silicon atom sites are covered by methyl group, and the surface passivation ratio can be defined to 90% accordingly. The ratio of pristine allyl terminated silicon surface is about 60% and the hybrid methyl/allyl terminated one is nearly 100%.

3.2. Device Structure. The device structure and the scheme of various surface passivations are illustrated in Scheme 1. The device is Schottky diode between the n-type Si and the PEDOT:PSS layer. Scheme 1 shows an ideal case of the hybrid structure. The thicknesses of different layers are not in real scale, the image of real device is shown in Figure S1 in the Supporting Information. Previous investigations indicated that the freshly prepared SiNWs with metal ion-assisted electroless etching are unsuitable for solid hybrid solar cells application because the polymer cannot penetrate far down into the gaps between the nanowires due to over dense wire arrays.[16,26] To overcome this issue, the density of SiNWs should decrease, and we have reported a simple method to tune the distance between adjacent wires.[4] The SEM images of dense and sparse SiNWs are shown in Figure S2 in the Supporting Information. According to our previous work, the expanded adjacent space between wires allows the PEDOT:PSS penetrate down to the bottom part of SiNWs and form a continuous film on SiNWs

Scheme 1. (a) Device Structure; (b) Scheme of Various Surface Terminations of Silicon: (i) Hydrogen Termination (with some dangling bonds); (ii) Methyl Termination (with some Si−H bonds and dangling bonds); (iii) Allyl Termination (with some Si−H bonds and dangling bonds); (iv) Hybrid Methyl/Allyl Termination (almost all Si−C bonds)

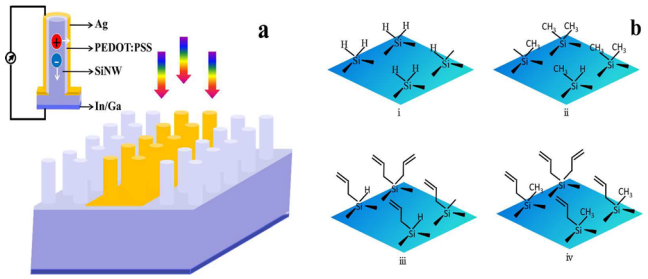

surface. In addition, the large distance between adjacent nanowires provides enough space where the anode is allowed deposit continuously in order to collect holes efficiently. In this work, the sparse SiNWs are utilized to fabricate hybrid devices. Figure 3 shows the TEM image of single wire coating with PEDOT:PSS layer. As shown in Figure 3, the PEDOT:PSS film wraps wire completely, and the film thickness is about 60 nm.

3.3. Electrical Output Characteristics of the Devices. The typical current density versus voltage ($J-V$) curves of the devices based on different organic monolayer passivated SiNWs are plotted in Figure 4. The electrical output characteristics are summarized in Table 2. The passivation layer plays critical role on the device performance. The device fabricated from allyl passivated SiNWs with short-circuit current density (J_{sc}) of 32.3 $mAcm^{-2}$, open circuit voltage (V_{oc}) of 0.512 V and fill factor (FF) of 0.57 yields a PCE of 9.4%, which is the lowest PCE in these three states of the surface passivations. In contrary, the device fabricated from methyl/allyl terminated SiNWs with J_{sc} of 32.6 $mAcm^{-2}$, V_{oc} of 0.514 V, and FF of 0.62 yields the highest PCE of 10.2%. Regarding the devices based on allyl-passivated SiNWs and methyl/ally ones, the low PCE mainly results from the low FF, which may be ascribed to the low monolayer organic coverage ratio (~60%) of allyl groups verified by XPS measurement. The uncovered sites with Si−H bonds or dangling bonds can be charge recombination center, which decrease the FF dramatically. For methyl and methyl/

dx.doi.org/10.1021/am302893r | ACS Appl. Mater. Interfaces 2013, 5, 4678−4684

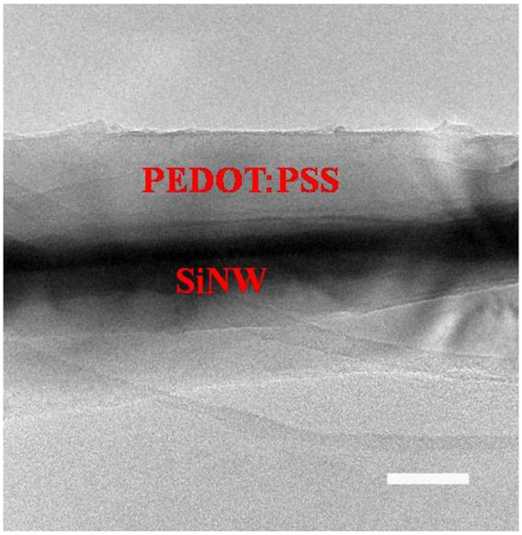

Figure 3. TEM image of a single wire coated with PEDOT:PSS film; the scale bar is 50 nm.

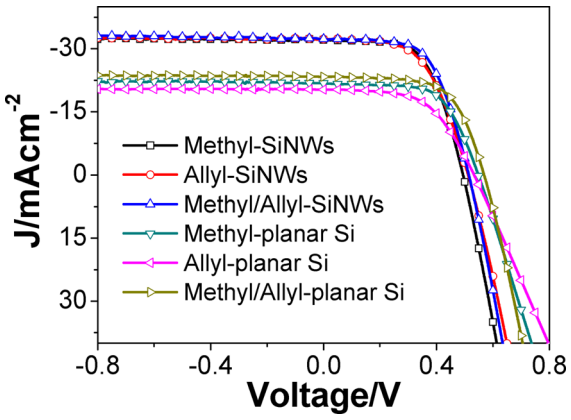

Figure 4. Electric output characteristics of hybrid devices based on planar Si and SiNWs with different surface passivations under simulated 1.5 A.M. solar illumination at 100 mW cm^{-2}.

Table 2. Electronic Output Characteristics of Hybrid Devices with the Different Surface Passivations

silicon structure	J_{sc} (mA cm^{-2})	V_{oc}/V	FF	PCE/%
methyl-planar-Si	21.8	0.548	0.63	7.6
allyl-planar-Si	20.3	0.533	0.56	6.1
methyl/allyl-planar Si	23.3	0.568	0.65	8.5
methyl-SiNWs	32.1	0.494	0.61	9.7
allyl-SiNWs	32.3	0.512	0.57	9.4
methyl/allyl-SiNWs	32.3	0.514	0.62	10.2

allyl terminated SiNWs based devices, the wires surfaces are almost completely covered. From the $J-V$ curves of these two devices, the device fabricated from methyl passivated SiNWs shows lower J_{sc} and V_{oc}, it may be related to the small surface dipole moment of methyl group.[27] The large positive surface dipole of methyl/allyl group can lead to improved internal electrical field, which could provide the charge separation drift driving force.

However, the device performance improvement is relatively small from methyl-terminated SINWs to methyl/allyl ones. To further verify the improved performance of device with hybrid surface passivation, the electrical output characteristics of several devices that are obtained in nominally identical condition are plotted in Figure S3 in the Supporting Information. The results indicate that the device fabricated from methyl/allyl terminated SiNWs always exhibited enhanced PCE. Planar silicon substrate with methyl/allyl groups passivation was also utilized to confirm the improved the device based on SiNWs one. The device structure and the fabrication process were as same as SiNWs ones. The results indicate that all the devices based on planar silicon substrates exhibit lower PCE, and methyl/allyl terminated substrate still achieve the champion PCE as summarized in Table 2. The lower PCE of planar-silicon based device mainly caused by decreased J_{sc}. The higher J_{sc} of SiNWs-based devices should be ascribed to their lower reflectivity. The reflectivity of SiNWs and planar silicon substrates are measured, as shown in Figure 5. The reflectivity of SiNWs substrate is lower than 10% among 300−1200 nm. In contrast, the reflectivity of planar one is about 40% among this range.

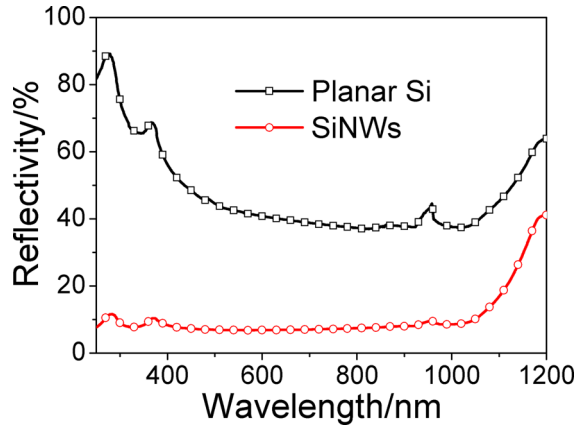

Figure 5. Reflectivity of planar silicon substrate and SiNWs one.

To explore the variation of electric output characteristic of device based on different surface passivation in-depth, the steady dark J-V curves are investigated and plotted in Figure 6. The dark $J-V$ curves of the SiNWs/PEDOT:PSS devices exhibit rectifying characteristics, and indicated that the SiNWs/PEDOT:PSS heterojunction behave as well-defined diodes.

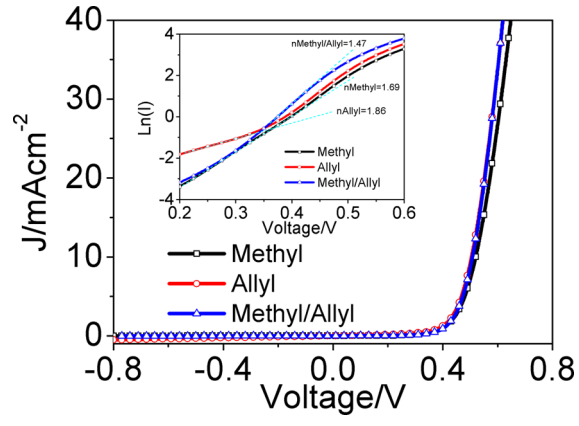

Figure 6. Electrical output characteristics of the devices with different surface passivations under dark condition and ln(I) versus voltage under dark condition showing diode ideality factors (inset).

dx.doi.org/10.1021/am302893r | ACS Appl. Mater. Interfaces 2013, 5, 4678−4684

The dark $J-V$ curves are simulated according to the diode equations

$$J = J_s\left(\exp\left(\frac{e}{nkT}V\right) - 1\right) \quad (1)$$

$$J_s = A^*AT^2\exp\left(-\frac{\Theta_{Bi}}{kT}\right) \quad (2)$$

Where A is the contact area, $A^*$is the effective Richardson constant [≈252 A cm^{-2} K^{-2} for n-type silicon], T is the absolute temperature (298 K), k is the Boltzmann constant, n is the diode ideality factor, J_s is the reversed saturation current density, and Φ_{bi} is the barrier height in Schottky diodes.

Equations 1 and 2 are often applied to evaluate the n value (the quality) of Schottky diodes.[9,28] According to eqs 1 and 2, the simulation curves are plotted in Figure 6 (inset Figure). The diode ideality factor and the barrier height are estimated, as illustrated in Table 3. The device based on hybrid methyl/allyl passivated SiNWs with the highest PCE of 10.2%, displays the smallest n, J_s and the highest Φ_{bi} values of 1.47, 4.46 × 10^{-5} mA cm^{-2} and 0.723 eV, respectively. The ideality factor is used to evaluate the charge carrier transport in the Schottky diode.[29] The case for n = 1 in the situation of a Schottky contact may be ascribed to voltage-dependent Schottky barriers because of image force lowering or interface states. The deviations from n > 1 may result from recombination currents within the space charge region or the thickness of depletion layer. In our work, the devices possess the same materials and the analogue structure, so we believe that these three devices should have the similar thickness of depletion layer. Because of the above reasons, the difference of the n value for our devices should be caused by the recombination. As shown in Table 3, the device based on allyl passivated SiNWs exhibits the largest n value of 1.86 and J_s of 3.43 × 10^{-4} mAcm^{-2}, which indicate that the serious charge recombination. The recombination results from the low coverage ratio of organic groups. In contrast, the device based on hybrid methyl/allyl passivated SiNWs shows the smallest n value of 1.47 and J_s of 4.46 × 10^{-5} mA cm^{-2}, which is caused by the complete surface passivation. The J_{sc} and V_{oc} are also enhanced with increasing the Φ_{bi}, which means that a large internal electric filed generated and the charge separation enhanced.

Table 3. Diode Ideality Factor (n), Reversed Saturation Current Density (J_s) and Schottky Barrier Height (Φ_{bi}) of Hybrid Devices with the Different Surface Passivations on the SiNWs

surface passivation	n	J_s (mA cm^{-2})	Φ_{bi}/eV
methyl-SiNWs	1.69	1.51 × 10^{-4}	0.692
allyl-SiNWs	1.86	3.43 × 10^{-4}	0.671
methyl/allyl-SiNWs	1.47	4.46 × 10^{-5}	0.723

Transient electric output characteristics measurements can be applied to characterize charge recombination kinetics in the hybrid solar cells at the open circuit condition.[30−33] The detailed processes and typical curves of the transient photovoltage and photocurrent measurements are illustrated in Figure S4 in the Supporting Information. The carrier concentration (N) for each open circuit voltage be obtained by integrating the capacitance over voltage

$$N = \frac{1}{Aed}\int_0^{V_{oc}} C\,dV \quad (3)$$

Where A is the device area, e is the electron charge, and d is the whole device thickness.

N is also the amount of excess carriers needed to separate the quasi-Fermi levels to the corresponding V_{oc}, which is mainly caused by the number midgap states that need to be filled.[33] Here, in our work, the SiNWs substrates are same type, so the midgap states should be same, the difference of the N value should be ascribed to the difference of the interface trap states. The N values versus V_{oc} of different passivated SiNWs/PEDOT:PSS devices are plotted in Figure 7. According to Figure 7, we can observe that the device based on methyl/allyl passivated SiNWs possesses the smallest density of trap states, which lead to the lowest J_s and n, which are illustrated in Table 3. In contrary, the device based on allyl passivated SiNWs possesses the largest density of trap states, which lead to the highest J_s and the smallest n. All the results are coordinated with the XPS measurement.

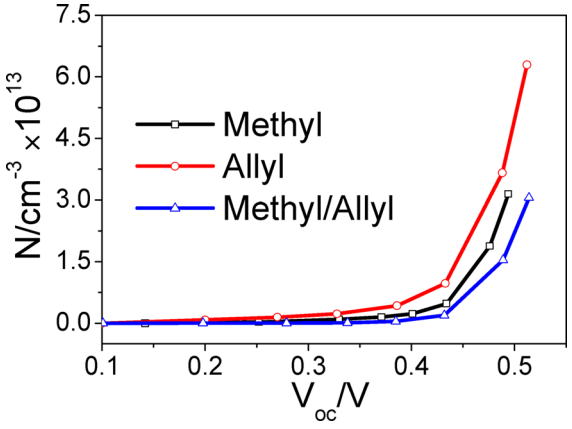

Figure 7. Number of density of trap states (N) versus open circuit voltage (V_{oc}) of the different passivated SiNWs/PEDOT:PSS devices.

The transient voltage decay also can be fitted with a monoexponential decay equation[30]

$$\Delta V = A\exp\left(-\frac{\tau}{T}\right) \quad (4)$$

Where A is a constant that fits to the peak height, τ is charge carrier lifetime, and T is the decay time constant. The carrier lifetimes we obtained here should be the effective carrier lifetimes, which including the carrier lifetime both at interface (τ_1) and inside the bulk Si (τ_2). Here, for our devices, the Si substrates are same, so the τ_2 should be the same value. The difference between the different devices should be caused by the τ_1, which was induced by the different surface passivation. In this technique, the interface trap states act as the charge recombination center only enhance the charge recombination velocity and can affect the carrier lifetimes, and the emission time constant of the interface traps is neglected. Here, in the measurement process, the pulse duration is set to 1 μs and the repetition rate to 100 Hz. The intensity of the pulsed laser is set so that the modulated V_{oc} is less than 10 mV. The background light intensity is set to 100 mW cm^{-2}, which are the same condition as the $J-V$ test. From the transient voltage decay fitting which are illustrated in Figure S5 in the Supporting Information, the charge carriers lifetime can be obtained and

are plotted in Table 4. The device fabricated from methyl/allyl passivated SiNWs shows the longest charge carrier lifetime of 2.93×10^{-5} s and the device fabricated from allyl passivated SiNWs shows the shortest charge carrier lifetime of 1.72×10^{-5} s. Generally, the traps in photovoltaic devices act as charge recombination centers. As shown in Figure 7, the device fabricated from methyl/allyl-passivated SiNWs shows the smallest n value, which is caused by the longest charge carrier lifetime. In contrast, the device based on allyl-passivated SiNWs possesses the largest n value, which resulted from the shortest charge carrier lifetime.

Table 4. Charge Carrier Lifetime of Hybrid Devices with the Different Surface Passivations on the SiNWs

device	τ (s)
methyl-SiNWs	2.45×10^{-5}
allyl-SiNWs	1.72×10^{-5}
methyl/allyl-SiNWs	2.93×10^{-5}

According to the XPS measurement, we can observe that all of these three passivation layer possess different coverage ratio. The uncovered site on the surface could be oxidized by oxygen and water in air with time elapsing, which can lead to the device degradation. The devices based on SiNWs with different passivation layer should exhibit different stability with time elapsing. The stability of the devices fabricated from different surface passivations with time elapsing are plotted in Figure S6 and summarized in Table S1 in the Supporting Information. After 240 h operation in air condition, the PCE of device fabricated from methyl/allyl-passivated SiNWs exhibits negligible decay. In contrary, the PCE of device fabricated from methyl-passivated SiNWs degrades from 9.7 to 9.3%. However, the FF of device fabricated from allyl-passivated SiNWs shows slight improvement. To investigate the reason for this phenomenon, we investigated the dark $J-V$ curves and plotted them in Figure S7 and summarized them in Table S2 in the Supporting Information. After 240 h of operation, the value of n and J_s of the hybrid methyl/allyl-passivated device show no change compared with the fresh one. In contrast, the value of n (J_s) of the methyl-passivated SiNW-based device increased dramatically from 1.69 (1.51×10^{-4} mA cm^{-2}) to 1.99 (9.85×10^{-4} mA cm^{-2}), respectively. With time elapsing, the uncovered sites at methyl passivated SiNWs could be oxidized and the natural oxidation of the SiO_x layer generated, which may become the charge transporting block layer due to its insulating properties. The value of n (J_s) of allyl passivated SiNW-based device decrease obviously from 1.86 (3.43×10^{-4}) mA cm^{-2} to 1.76 (2.44×10^{-4}) mA cm^{-2}, respectively. For allyl terminated surface, there are lots of dangling bonds or Si−H bonds on the surface initially, which leads to the most seriously charged recombination. With time elapsing, the uncovered area with dangling bonds or Si−H bonds change into ultrathin SiO_x layer, which could suppress the charge recombination velocity and enhance the device performance.

4. CONCLUSION

In conclusion, we have demonstrated that hybrid Schottky junction solar cells based on organic methyl/allyl monolayer passivated SiNWs and PEDOT:PSS display an improved PCE of 10.2% and excellent stability. From transient and steady electrical output characteristics measurements, the surface passivation of SiNWs plays critical role on the device performance because it dominated the charge recombination process. In addition, the device fabricated from methyl/allyl-passivated SiNWs shows better stability than those based on pristine methyl- and allyl-passivated ones. The high PCE and good stability of the device is ascribed to the excellent functionalization of the SiNWs surface. The Schottky junction between SiNWs and PEDOT:PSS was formed by a simple solution-processed method at a temperature as low as 110 °C, which could avoid the degradation of Si quality in the high-temperature fabrication processes. This investigation indicates that stable organic/inorganic hybrid PV devices with a high PCE could be achieved by facile processes and may be a technology alternative for traditional silicon solar cells.

■ ASSOCIATED CONTENT

Supporting Information

The real device image, SEM images of SiNWs, the performance variation of devices based on SiNWs, photovoltage transient technique, electric output characteristics under dark, and illumination of devices after operation in air for 240 h. This material is available free of charge via the Internet at http://pubs.acs.org/.

■ AUTHOR INFORMATION

Corresponding Author

*E-mail: bqsun@suda.edu.cn. Tel: 0086-512-65880951.

Notes

The authors declare no competing financial interest.

■ ACKNOWLEDGMENTS

This work was supported by the National Basic Research Program of China (973 Program) (2012CB932402), National Natural Science Foundation of China (91123005, 61176057, 61211130358, 60976050), and the Priority Academic Program Development of Jiangsu Higher Education Institutions.

■ REFERENCES

(1) Lewis, N. S.; Nocera, D. G. *Proc. Natl. Acad. Sci. U.S.A.* **2006**, *103*, 15729−15735.
(2) Green, M. *Sol. Energy* **2004**, *76*, 3−8.
(3) Zhang, F.; Sun, B.; Song, T.; Zhu, X.; Lee, S. *Chem. Mater.* **2011**, *23*, 2084−2090.
(4) Zhang, F.; Han, X.; Lee, S.; Sun, B. *J. Mater. Chem.* **2012**, *22*, 5362−5368.
(5) Tsai, S. H.; Chang, H. C.; Wang, H. H.; Chen, S. Y.; Lin, C. A.; Chen, S. A.; Chueh, Y. L.; He, J. H. *ACS Nano* **2011**, *5*, 9501−9510.
(6) Shen, X.; Sun, B.; Liu, D.; Lee, S. T. *J. Am. Chem. Soc.* **2011**, *133*, 19408−19415.
(7) Jeong, S.; Garnett, E. C.; Wang, S.; Yu, Z.; Fan, S.; Brongersma, M. L.; McGehee, M. D.; Cui, Y. *Nano Lett.* **2012**, *12*, 2971−2976.
(8) He, L.; Jiang, C.; Lai, D.; Wang, H. *Appl. Phys. Lett.* **2011**, *99*, 021104.
(9) Fan, G.; Zhu, H.; Wang, K.; Wei, J.; Li, X.; Shu, Q.; Guo, N.; Wu, D. *ACS Appl. Mater. Interfaces* **2011**, *3*, 721−725.
(10) Groenendaal, L.; Jonas, F.; Freitag, D.; Pielartzik, H.; Reynolds, J. R. *Adv. Mater.* **2000**, *12*, 481−494.
(11) Kirchmeyer, S.; Reuter, K. *J. Mater. Chem.* **2005**, *15*, 2077−2088.
(12) He, L.; Jiang, C.; Wang, H.; Lai, D. *IEEE Electron Device Lett.* **2011**, *32*, 1406−1408.
(13) Lu, W.; Wang, C.; Yue, W.; Chen, L. *Nanoscale* **2011**, *3*, 3631−3634.
(14) Ono, M.; Tang, Z.; Ishikawa, R.; Gotou, T.; Ueno, K.; Shirai, H. *Appl. Phys. Express* **2012**, *5*, 2301.

(15) Shiu, S. C.; Chao, J. J.; Hung, S. C.; Yeh, C. L.; Lin, C. F. *Chem. Mater.* **2010**, *22*, 3108−3113.
(16) Zhang, F.; Song, T.; Sun, B. *Nanotechnology* **2012**, *23*, 194006.
(17) Chen, T.-G.; Huang, B.-Y.; Liu, H.-W.; Huang, Y.-Y.; Pan, H.-T.; Meng, H.-F.; Yu, P. *ACS Appl. Mater. Interfaces* **2012**, *4*, 6857−6864.
(18) Amy, S. R.; Michalak, D. J.; Chabal, Y. J.; Wielunski, L.; Hurley, P. T.; Lewis, N. S. *J. Phys. Chem. C* **2007**, *111*, 13053−13061.
(19) Buriak, J. M. *Chem. Rev.* **2002**, *102*, 1271−1308.
(20) O'Leary, L. E.; Johansson, E.; Brunschwig, B. S.; Lewis, N. S. *J. Phys. Chem. B* **2010**, *114*, 14298−14302.
(21) Vilan, A.; Yaffe, O.; Biller, A.; Salomon, A.; Kahn, A.; Cahen, D. *Adv. Mater.* **2009**, *22*, 140−159.
(22) Puniredd, S. R.; Assad, O.; Haick, H. *J. Am. Chem. Soc.* **2008**, *130*, 13727−13734.
(23) Pritchard, H.; Skinner, H. *Chem. Rev.* **1955**, *55*, 745−786.
(24) Johansson, E.; Boettcher, S. W.; O'Leary, L. E.; Poletayev, A. D.; Maldonado, S.; Brunschwig, B. S.; Lewis, N. S. *J. Phys. Chem. C* **2011**, *115*, 8594−8601.
(25) Peng, K. Q.; Yan, Y. J.; Gao, S. P.; Zhu, J. *Adv. Mater.* **2002**, *14*, 1164−1167.
(26) Greene, L. E.; Law, M.; Yuhas, B. D.; Yang, P. *J. Phys. Chem. C* **2007**, *111*, 18451−18456.
(27) Maldonado, S.; Plass, K. E.; Knapp, D.; Lewis, N. S. *J. Phys. Chem. C* **2007**, *111*, 17690−17699.
(28) Li, X.; Zhu, H.; Wang, K.; Cao, A.; Wei, J.; Li, C.; Jia, Y.; Li, Z.; Wu, D. *Adv. Mater.* **2010**, *22*, 2743−2748.
(29) Werner, J. H. *Appl. Phys. A−Mater.* **1988**, *47*, 291−300.
(30) Li, Z.; Gao, F.; Greenham, N. C.; McNeill, C. R. *Adv. Funct. Mater.* **2011**, *21*, 1419−1431.
(31) Shuttle, C.; ORegan, B.; Ballantyne, A.; Nelson, J.; Bradley, D.; De Mello, J.; Durrant, J. *Appl. Phys. Lett.* **2008**, *92*, 093311.
(32) Koleilat, G. I.; Levina, L.; Shukla, H.; Myrskog, S. H.; Hinds, S.; Pattantyus-Abraham, A. G.; Sargent, E. H. *ACS Nano* **2008**, *2*, 833−840.
(33) Ip, A. H.; Thon, S. M.; Hoogland, S.; Voznyy, O.; Zhitomirsky, D.; Debnath, R.; Levina, L.; Rollny, L. R.; Carey, G. H.; Fischer, A. *Nat. Nanotechnol.* **2012**, *7*, 577−582.